Effects of Major Errors Sources on Planetary Spacecraft Navigation Accuracies

JAMES F. JORDAN,* GEORGE A. MADRID,† AND GERALD E. PEASE‡
Jet Propulsion Laboratory, Pasadena, Calif.

Tighter accuracy requirements on future planetary missions, than on past missions, make it desirable to improve 1) the accuracy of real-time state estimates and 2) the reliability of preflight state estimate error statistics. This paper is addressed to the second problem area. The sources of the major errors in the Earth-based tracking system are listed and discussed, and the effects of these errors on the predicted spacecraft orbit determination accuracies for two future interplanetary missions are presented.

Nomenclature

a = v_r, geocentric radial velocity of the probe
b = $\omega r_s \cos\delta_o$
c = $\omega r_s(\Delta\alpha - \Delta\lambda)\cos\delta_o$
ω = rotation rate of the Earth
r_s = station's distance from the Earth's spin axis
δ_o = geocentric declination of the probe
$\Delta\alpha$ = deviation in geocentric right ascension from nominal
$\Delta\lambda$ = deviation in tracking station longitude from nominal
$\dot{\rho}$ = spacecraft-station range rate
μ = mass constant of the sun
V = (3×1) spacecraft velocity vector
X = (3×1) spacecraft position vector
$x'(t)$ = (6×1) estimate of state deviations given data to time t
F = (6×6) matrix $\{= \partial[(-\mu/r^3)\,X,V]/\partial(V,X)\}$
H = (1×6) matrix $[= \partial\dot{\rho}/\partial(V,X)]$
Λ = (6×6) covariance matrix of the error in $x'(t)\{= E[(x - x')(x - x')^T]\}$
R = $\sigma_e^2 \Delta t$
σ_e = standard deviation of the error in each range rate measurement due to noise
Δt = the time interval between which data are taken
r = probe-sun distance, in km
k = 1.0088×10^8, a solar radiation constant
A = spacecraft effective area normal to **R**, nominally 11.0 m^2 for MM'71 spacecraft
M = spacecraft mass, nominally 980 kg for MM'71 spacecraft
G_R = reflectivity coefficient
G_X = Ax/A, where A_x is the effective spacecraft area normal to **X**
G_Y = Ay/A, where A_y is the effective spacecraft area to normal **Y**
R = unit vector directed out from sun to spacecraft
X = unit vector corresponding to the spacecraft $+x$ direction (pitch axis)
Y = unit vector corresponding to the spacecraft $+y$ direction (yaw axis)
η = (3×1) vector disturbing acceleration
q = vector error in the observation
E = $F - KH$ (a 6×6 matrix)
C = $E[\eta(x - x')^T]$
D = $E[q(x - x')^T]$
H_1 = $\partial\dot{\rho}/\partial q$

Presented as Paper 70-1077 at the AAS/AIAA Astrodynamics Conference, Santa Barbara, Calif., August 19–21, 1970; submitted October 7, 1970, revision received October 1, 1971. This paper represents one phase of research carried out at the Jet Propulsion Lab., California Institute of Technology, under NASA Contract NAS 7-100.

Index categories: Spacecraft Navigation, Guidance, and Flight Path Control Systems; Spacecraft Tracking.

* Group Supervisor, Precision Orbit Determination Group.
† Senior Research Engineer, Navigation Accuracy Group.
‡ Senior Research Engineer, Estimation Theory Group.

Introduction

THE principal navigation system for planetary missions employs observations of the doppler shift in a coherent two-way radio signal between Earth-based tracking stations and the spacecraft. The capabilities and limitations of this system are outlined by Hamilton.[1] Although the use of the system has resulted in highly successful Mariner missions in the 1960's, in many cases, the predicted accuracy of state estimates, based only on statistics of the data noise, has been better than that encountered during real-time flight operations.

The effects of some of the major error sources on the navigation accuracies achievable with current data processing tools are presented in this paper. The information content of Earth-based doppler data is discussed and the equations for the spacecraft state estimate and the covariance matrix of the error in the estimate are set forth in the continuous data filter formulation. The sources of major errors in the Earth-based tracking systems are listed, and the effects of these errors on the interplanetary (pre-encounter) phases of the Mariner missions to Mars in 1971 and Venus-Mercury in 1973 are presented.

Earth-Based Spacecraft Orbit Determination and Accuracy Analysis

It has been shown[2] that the station-spacecraft range-rate over a pass of tracking data can be approximately related to slowly varying parameters a, b, and c by the following relation if epoch time is taken at the center of the pass:

$$\dot{\rho} = a + b\sin\omega t + c\cos\omega t \qquad (1)$$

From the analysis of a single pass of tracking data, the parameters a, b, and c, and hence, the geocentric range-rate of the spacecraft, its geocentric right ascension, and the cosine of its declination can be estimated. By combining successive passes of range-rate data, changes in the parameters, a, b, and c can be noted, which in turn relate to the spacecraft radial acceleration, the velocity in the right ascension direction, and the velocity in the declination direction.[3] Using the sun-Earth-spacecraft geometry, the radial acceleration can be related to the Earth-spacecraft range. Thus, the entire state (position and velocity) of a distant spacecraft can be determined from a few passes of doppler data. If many passes of data are obtained, the spacecraft state can be estimated so well that this data type currently constitutes the principal navigation observable for planetary missions. A large scale computer program, the Double Precision Orbit Determination Program (DPODP), is currently operated by JPL to process range-rate data from the Deep Space Network tracking stations and generate estimates of the spacecraft state at desired epochs.

If the accuracy of the range-rate observables is limited only by data noise, and the spacecraft trajectory obeys two-body equations of motion then the estimate of the state deviations from a nominal trajectory obeys the following differential equation from Kalman filtering theory[4]

$$\dot{x}' = Fx' + K(\Delta\dot{\rho} - Hx') \tag{2}$$

where K is a weighting matrix which will be defined subsequently. The covariance matrix of errors in the state estimate computed from Eq. (2) obeys the well-known matrix Riccati equation

$$\dot{\Lambda} = F\Lambda + \Lambda F^T - \Lambda H^T R^{-1} H\Lambda \tag{3}$$

The optimal weighting matrix for a minimum variance state estimate can now be stated as

$$K(t) = \Lambda(t)H^T(t)R^{-1} \tag{4}$$

Although DPODP does not use the continuous data filter formulation presented here, but employs discrete batch-processor computational algorithms, this program generates state estimate and associated statistics which are theoretically identical to the solutions of Eqs. (2) and (3).

Major Errors Affecting Navigational Accuracy

There are three major types of errors which affect navigational accuracy. These are observer-related errors, spacecraft-related errors, and ephemeris errors. The first of these occurs through the use of insufficiently accurate models to locate the observer in inertial space and to calibrate out the effects of the transmission media. The second type occurs through imprecise modeling of the accelerating forces on a spacecraft. The last type is due to an imprecise model for the inertial position of the planets.

Observer-Related Errors

The observer-related error sources which contribute significantly to the composition of the noise signature on radio tracking data can be classified into two main categories. The first consists of errors in locating the tracking station with respect to inertial space and includes DSS locations with respect to the Earth's crust, polar motion, and variation in Earth rotation rate (Time variations). The second category consists of errors that corrupt the information content of the observation and includes the effects of charged particles in the space plasma and the Earth's ionosphere, refractive effects in the Earth's troposphere, station equipment signal delay, station oscillator instability and synchronization. A brief description of the physical aspects of each of these error phenomena follows. (Station Equipment errors omitted.)

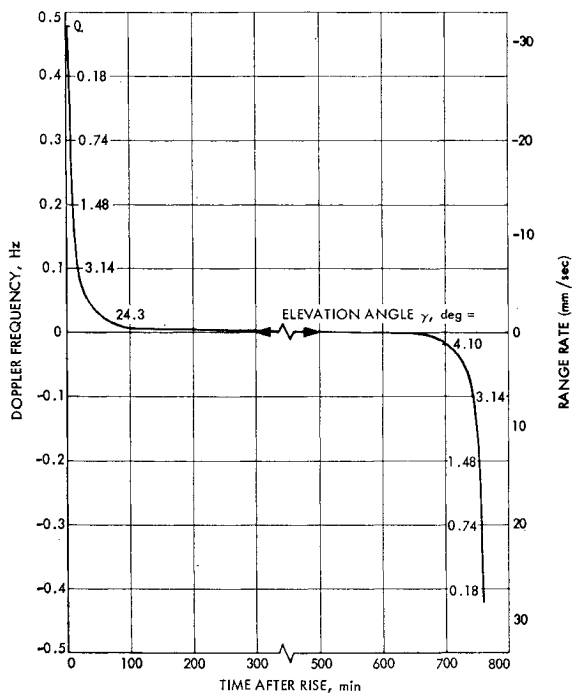

Fig. 1 Correction for tropospheric doppler and range-rate effects.

Tropospheric Effects

The refractive effect of the troposphere retards and bends an electromagnetic signal making the observation appear as if the beam had traveled through a longer distance. This difference is such that radio measurements of range-rate are significantly affected. Figure 1, due to Liu,[5] shows the correction that must be made to compensate for the dry refractive component.§ The wet component for the refractive effect has not been adequately modeled but it's behavior is nearly uncorrelated and random. This unmodeled portion of the refractive effect occurs with a relatively high frequency and yields range rate variations having a standard deviation of about 0.3 mm/sec at 10° elevation.

Charged Particle Effects

The radio signals traveling between a station and a spacecraft pass through the interplanetary space plasma, the ionosphere of the Earth, and possibly the ionosphere of other planets. The interaction between the radio signal and the charged particles in the medium causes, among other phenomena, a change in the ray path length. The group path length is increased while phase path length is decreased by the presence of charged particles. As the density of charged particles varies, the resultant time rate of change in the phase path length corrupts doppler measurements made from the radio signal.

The Earth's ionosphere is caused by ultraviolet light from the sun, ionizing the upper atmosphere. Consequently, the ionosphere above a tracking station increases and decreases with roughly a diurnal period. If the ionospheric effect is not measured or modeled, it cannot be easily distinguished from errors in tracking station location, and may result in significant errors for in-flight orbit determination.

The effects of charged particles in the ionosphere can be detected by measuring the rotational effect (Faraday rotation) on a linearly polarized radio signal or by ionosonde readings. The Faraday rotation measurements are usually made by examining the signal from geostationary satellites (e.g., the Applications Technology Satellites). The polarization of the ATS signal is continuously measured, digitized, and recorded. By processing this information a measurement of electron content can be obtained and used to calibrate the Earth's ionosphere over a complete diurnal cycle. Corrections to spacecraft tracking data require the mapping of the electron content to the spacecraft line of sight and the computation of the doppler corrections.

§ The JPL model for calibrating the dry refractive effects is based on an assumption of an isotropic, isothermal atmosphere.[6] An empirical formula is used to present the ray-traced effects of this model. The range rate form of this expression is:

$$\Delta\dot{\rho} = A\left\{\frac{1}{[\sin\lambda(t_{ob}) + B]^{1.4}} - \frac{1}{[\sin\lambda(t_{ob} - \tau) + B]^{1.4}}\right\}$$

where A is a constant dependent on the transmission frequency, λ is the elevation angle of observation, τ is the doppler averaging time, t_{ob} is the time of observation, and $B = 0.06483$. Note: the "dry" refraction component refers to those effects due to an atmosphere with zero water vapor. The "wet" designation refers to the added refractivity due to water vapor.

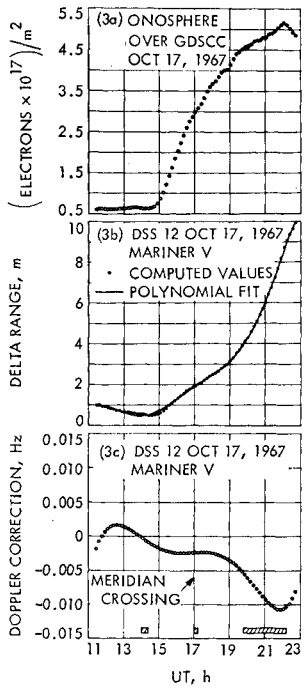

Fig. 2 Mariner V ionospheric effects as they relate to range and range rate.

Ionosonde measurements are obtained from instruments dedicated to this purpose which transmit radio signals vertically into the ionosphere. By repeatedly transmitting signals of increasingly higher frequency a particular frequency is found which is no longer reflected but which pierces the ionosphere. By measuring the elapsed time for each reflected frequency the altitude dependence of the electron density can be determined up to the altitude of the piercing frequency.

Figure 2, due to Mulhall,[7] illustrates how electron content obtained through the use of a Faraday rotation device can be mapped to yield a range effect and thence to a doppler effect. Maximum effects of close to 1 mm/sec (0.015 hz) are approached throughout the year. Figure 3, (Ref. 7) shows similar effects for space plasma. On the day shown, the space plasma effects had peaks of 22 m in range and 01.6 mm/sec in doppler, both of which are almost twice as large as that produced by an average active ionosphere.[8]

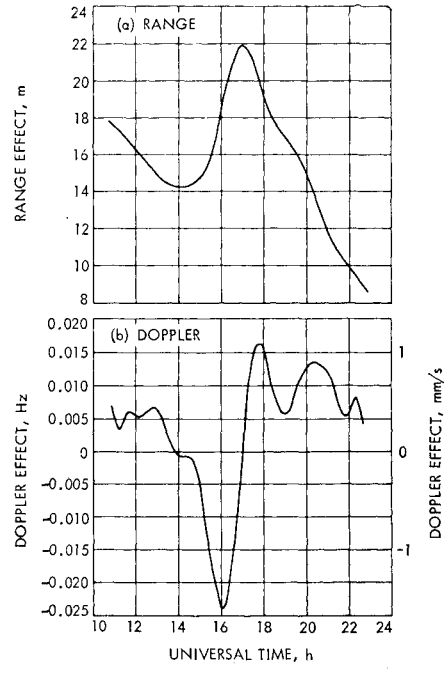

Fig. 3 Mariner V space plasma range and doppler effects on October 31, 1967.

Timing Errors

Trask and Muller[9] have demonstrated that timing errors can cause a degradation in the quality of the tracking data used for orbit determination. These errors arise in any of the five timing systems used in the orbit determination process. Ephemeris Time (ET) is used to look up the position of the sun and the planets; (UT1) is used to determine the location of a tracking station in space; Station time (ST) is used to take the actual observational data. Ephemeris Time is a uniform mathematical measure of time approximated on Earth by Atomic Time (A.1). Station Time is related to Universal Time (UTC), which in turn is related to (A.1). (UT1) however, is not uniform since it depends on the rotational motion of the Earth. Thus, if the station's position were computed using (ST), which is only an approximation to Universal Time, an error would be introduced because the actual geocentric position of the station would not correspond to that used in the model.

To correct for this situation the differences between A.1 and UT1 are plotted for long period of time and the expected differences extrapolated by polynomials for the times of interest. According to current estimates, predicted time values utilizing these corrections should not deviate by more than 5.0 msec from the true value, over a weekly extrapolation. This error can result in a 2 m range error or 0.02 mm/sec range rate error.

Polar Motion

The motion of the Earth's axis of figure with respect to the spin axis is termed polar motion. This motion can be conceived as the change of position of that point on the Earth's crust through which the spin axis passes. In no way, however, does this imply that the position of the spin axis is changing in inertial space, rather, it corresponds to a change of the Earth's crust with respect to the spin axis.

The International Polar Motion Service (IPMS) and the Bureau International de l'Heure (BIH) are charged with observing and documenting polar motion. By extrapolating the data over weekly intervals and converting it to effects of the location of tracking stations, attempts can be made to correct for this effect. Range rate errors in these corrections do not exceed 0.03 mm/sec.

DSS Location Errors

Uncertainties in the distance of a tracking station from the Earth's spin axis and in station longitude can have a major effect on encounter orbit determination accuracies. The uncertainty in the tracking station location parallel to the spin axis does not introduce a significant error in the range rate observable, although an error in the spin axis distance (r_s) is directly related to the predicted probe position in the declination direction, and an error in longitude (λ) affects the right ascension, both of which are normal to the Earth-probe direction. These effects can be seen in the definitions accompanying Eq. (1).

The uncertainties in tracking station locations stem mainly from pole wandering and actual motion of the Earth's crust relative to itself. Estimates of previous station locations are obtained through post-flight analysis of previous missions. These estimates are updated for current use by correcting them for polar motion. The currently accepted mean amplitude of the variations in the solution for spin axis and longitude is 3 m[10]. The variations in r_s and λ have a very long period and would cause a maximum change in the nominal doppler amount to 0.0015 Hz or about 0.1 mm/sec.

Spacecraft Related Errors

Spacecraft navigational errors due to nongravitational forces can be classified according to their source either as spacecraft generated forces or as spacecraft interactions with its environment. The first category includes forces which occur during a spacecraft's operation and which are internal to the spacecraft; this includes gas leaks, and attitude thruster unbalance. The second type of forces arise from the spacecraft's interaction with its environment such as solar pressure. The discussion in this paper will restrict itself to cold gas leakages and solar radiation pressure.

Gas Leakage

The effect of gas leakage on some previous Mariner missions has been a major limiting factor on the navigation accuracy. These accelerations arise from imperfect seat tolerances on the gas valves of the attitude control system and from fuel leaks from the midcourse guidance engine. Little is known about the nature of these forces other than approximations to their magnitude which are between 10^{-12} km/sec^2 abd 10^{-11} km/sec^2 (Ref. 11). The accelerations are believed to be nearly constant over much of a missions duration.

Solar Radiation Pressure

Solar Radiation pressure is presently modeled by the following equation

$$\Delta\ddot{\mathbf{R}} = (kA/Mr^2)\,(G_R\mathbf{R} + G_X\mathbf{X} + G_Y\mathbf{Y}) \qquad (5)$$

During the Mariner V mission to Venus estimates were made of the solar radiation pressure coefficients.[12] A distinct trend towards lower pressure with increasing time was evident. This was attributed to a decrease of the spacecraft's reflectivity rather than an actual decrease in solar radiation pressure. The variation in G_R was between 0.4 and 0.36 over the life of the mission, which corresponds to a 3% slowly varying uncertainty in solar force of about 0.15 dyne. This is about 6×10^{-12} km/sec^2 in acceleration. Mars missions should endure an uncertainty closer to only 1×10^{-12} km/sec^2 due to increased heliocentric range.

Planetary Ephemeris Errors

The accuracy to which a spacecraft can be navigated to a planet depends not only on the accuracy to which Earth-tracking and spacecraft errors can be modeled but also depends on the precision with which the target planet can be located. The current JPL ephemerides can accurately predict the location of Mars to within 10 km in-plane and 50 km out-of-plane.[13] Venus can be located to within 5 km in-plane and 10 km out-of-plane. These accuracies are, of course, all relative to the position of the Earth in space.

Analysis of the Sensitivity of the Navigation Accuracy to the Major Unmodeled Errors

The major unmodeled sources of error in the spacecraft state estimates computed on the basis of range-rate data are the physical station location uncertainties, the effects due to charged particles in the Earth's ionosphere and the space plasma, and the effects of nongravitational accelerations acting on the spacecraft. The balance of the unmodeled error sources, which include station equipment parameters, the wet component of the troposphere refraction effect, and the residual timing and polar motion errors introduce a high-frequency noise on the range rate data with a standard deviation of less than or equal to 1 mm/sec. In order to simplify the following analysis, those unmodeled effects which exhibit high-frequency variations of 1 mm/sec or less will be considered jointly as 1 mm/sec "data noise." A conservative estimate of the effects of high-frequency errors on the state estimate accuracy can therefore be seen directly from the covariance matrix found from integration of Eq. (3), with $\sigma_\epsilon = 1$ mm/sec. The effect of the low-frequency errors on the tracking estimation system can be ascertained from the solution of the following sensitivity analysis equations:

If the true equations of motion of the spacecraft are

$$\dot{V} = (\mu/r^3)\,X + \eta \qquad \dot{X} = V \qquad (6)$$

and if the true data deviations from nominal are given as follows

$$\Delta\dot{\rho} = Hx + H_1\,q + \epsilon \qquad (7)$$

where q is the vector error, then the true covariance matrix Λ_c, of the error in the estimate derived from Eq. (2) obeys the differential equation

$$\dot{\Lambda}_c = E\Lambda_c + \Lambda_c E^T + KRK^T + C + C^T - KH_1D - D^TH_1{}^TK^T \qquad (8)$$

The continuous formulation of the sensitivity analysis equations was first presented by Sage and Griffin,[14] and has since been developed for application to the Earth-based orbit determination problem at JPL. In order to consider the four low-frequency error sources as disturbing phenomena in the equations, the errors η and q, must be described as appropriate stochastic processes whose autocorrelation function is prescribed. The following paragraphs list the four error sources, the properties of the assumed stochastic process describing each, and the partial derivative of the range-rate with respect to each error, which becomes H_1 in Eq. (8).

The uncertainties in the stations distance from the Earth's spin axis r_s and the longitude of the station λ will be described as constants for a particular mission. By using Eq. (1), the partial derivative matrix of the data with respect to r_s and λ can be calculated in terms of the nominal Earth-probe geometry as

$$\partial\dot{\rho}/\partial(r_s,\lambda) = (\omega\cos\delta_0\sin\omega t, -\omega r_s\cos\delta_0\cos\omega t) \qquad (9)$$

The effective path length variation due to the change in the number of charged particles in the ionosphere at any time is dependent on the instantaneous time of day and probe-station elevation angle. Since these variables, as well as the station locations, introduce diurnal signatures in the tracking observable $\dot{\rho}$, it is convenient to characterize the ionosphere effect as equivalent station location errors.[15] Figure 4 shows plots of

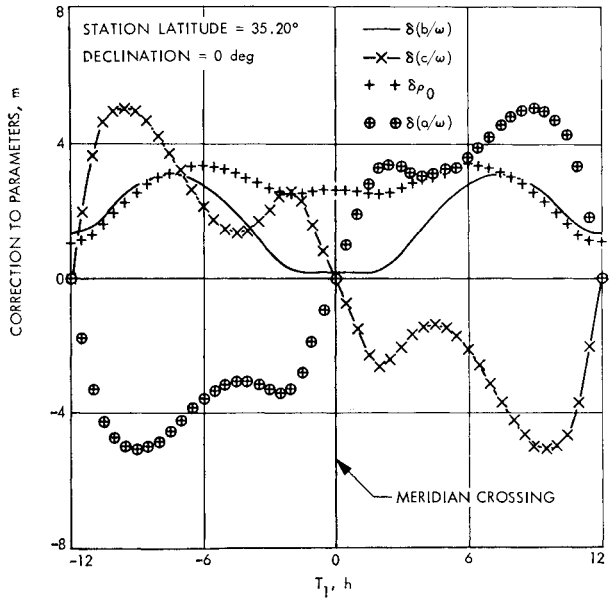

Fig. 4. Estimates of parameters a, b, a, and ρ_0 from Faraday rotation ionosphere measurements.

estimates of the errors induced in the parameters defined in Eq. (1) and the range at the center of the pass, i.e., $\Delta a/\omega$, $\Delta b/\omega$, $\Delta c/\omega$, and $\Delta\rho_o$, derived from the charged particle effect of a homogeneous ionosphere. The plots, which are due to Ondrasik et al,[15] show parameter estimates vs the sun-Earth probe angle in hours for $\delta_o=0$. The equivalent station error can be derived from the parameter error estimates in the equations

$$\Delta r_s=(1/\cos\delta_0)\Delta b/\omega \qquad \Delta\lambda=(-1/r_s\cos\delta_0)\Delta c/\omega \qquad (10)$$

Δa and $\Delta\rho_o$ must also be considered if the complete effect is included, although $\Delta\rho_o$ does not affect the Doppler data. The partial derivatives matrix of the data with respect to Δa, Δr_s, $\Delta\lambda$, and $\Delta\rho_o$ is

$$\partial\dot{\rho}/\partial(a,r_s,\lambda,\rho_o)=(1,\omega\cos\delta_o\sin\omega t,-\omega r_s\cos\delta_o\cos\omega t,0) \qquad (11)$$

The effective path length variation due to the change in the number of charged particles in the space plasma at any time is not dependent on any Earth related variables. Hence the effect can be modeled by a random process additive to the slowly varying parameter a. For simulation purposes, the modeled random process is assumed stationary, and exponentially autocorrelated in time. Spectral Analysis of Mariner V space plasma effects, obtained from dual frequency measurements and Faraday rotation data, leads to an estimated standard deviation for the effect of 0.16 mm/sec and a correlation time of 2 hr. For the space plasma error, $\partial\dot{\rho}/\partial a=1$.

Small accelerations due to all the nongravitational forces are also modeled as exponentially correlated noise. The specifications for leaks on future missions prescribe acceleration magnitudes to be less than 5×10^{-12} km/sec^2. Correlation times are expected to be very long; hence, the random acceleration can be considered to be nearly a bias.

If B_η is a diagonal matrix of the reciprocals of the correlation times of the random acceleration vector, and B_q is a diagonal matrix of observer related error correlation time reciprocals, then the matrices C and D obey the following equations

$$\dot{C}=B_\eta C+C\,E^T+R_\eta$$
$$\dot{D}=B_q D+D\,E^T-R_q H_1{}^T K^T \qquad (12)$$

where R_η and R_q are the respective covariance matrices of the acceleration and observer related errors.

Note that if an error source is assumed constant then the corresponding element of B_η or B_q is set to zero. Note, also, that since the a priori state estimate is uncorrelated with the error sources, the initial elements of C and D are zero. The preceding set of equations is programmed for the Univac 1108 computer at JPL. The program name is the Continuous Linear Orbit Determination Program (CLOD). Numerical results from the program compare well with those from both the DPODP and ODAC, a recently developed error analysis program for near-encounter orbit determination.[16]

Results for Mariner Mars '71 and Venus-Mercury '73

As a practical result of the above analysis, we now show how such an error model may be used to predict the target errors on two future JPL planetary missions, Mariner Mars 1971 and Mariner Venus-Mercury 1973. Specifically, we will examine the effects of the previously mentioned error sources on the orbit determination process in the 30 days preceding planetary encounter (Venus encounter in the case of MVM'73).

The ecliptic geometry of the 30 day tracking interval chosen for the two missions is shown in Fig. 5. The heliocentric arcs subtended by Earth and by the two spacecraft in these 30 day intervals are shown in ecliptic x and y coordinates. The geometry is especially interesting as a contrast between the relative importance of the ionospheric and space plasma effects, since in the case of Mariner '71 we are looking towards the sun, and on the Mars mission, away from it.

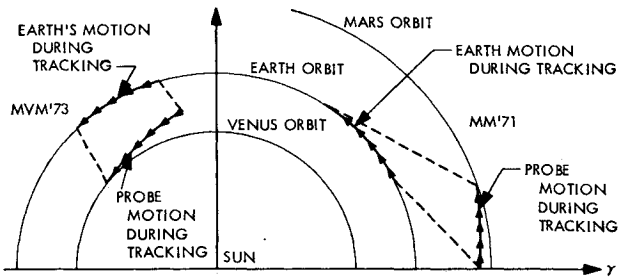

Fig. 5 Profile of Mariner Mars 1971 and Mariner Venus-Mercury 1973 pre-encounter tracking geometries.

Results are expressed in the B-plane system used at JPL to describe lunar and planetary miss distances.[17] B is the vector from the target's center of mass to the incoming asymptote of the spacecraft's planet-centered hyperbolic trajectory. The orientation of B in the plane normal to the direction of the incoming asymptote is described in terms of two unit vectors R and T. T is parallel to a fixed reference plane, in this case the ecliptic plane.

The statistical information contained in both the ideal covariance matrix Λ and the true covariance matrix Λ_c may be mapped to time of closest approach to the target planet and projected as a two-dimensional error ellipse on the B-plane. We employ a mapping matrix,

$$U(t,t_o)=\partial[V(t),X(t)]/\partial[V(t_o),X(t_o)]$$

where t_o and t are, respectively, the times at the end of the tracking span and at encounter.

The covariance matrix at encounter time t is then

$$\Lambda(t)=U(t,t_o)\Lambda(t_o)U^T(t,t_o)$$

The 1σ position error ellipse in the B-plane is described here in terms of its semimajor axis, SMAA, and semiminor axis SMIA, and orientation angle θ measured clockwise from T as viewed from the incoming asymptote. Note that the gravitational attraction of the encounter planet does not influence the B-plane dispersion ellipse, if tracking is terminated before the spacecraft motion is significantly influenced by the planet.

Statistics vs Tracking Span for Station Location and Acceleration Uncertainties

Figures 6 and 7 plot SMAA as a function of tracking time, starting 30 days before encounter, for the following models.

Curve 1: The only error source is a $\dot{\rho}$ data weight of $\sigma_\epsilon=1$ mm/sec per 60 sec sample. This weight encompasses receiver noise oscillator instability, and unmodeled tropospheric refraction errors, but assumes the location of the single tracking station is perfectly modeled over a 12 hr pass width. All other error sources, space plasma, ionospheric refraction, and nongravitational spacecraft accelerations are also assumed perfectly modeled.

Curve 2: This plot contains the effects of data weighting of 1 mm/sec per 60 sec sample and station location uncertainties. The standard deviations of the uncertainties are given as $\sigma_{r_s}=1.5$ m, $\sigma_\lambda=3.0$ m in 1971 (Fig. 7) and $\sigma_{r_s}=0.8$ m, $\sigma_\lambda=1.6$ m in 1973 (Fig. 8). Polar motion and timing errors are represented in this curve, but not the effects of charged particles or nongravitational spacecraft accelerations.

Curve 3: This plot demonstrates the effect of a spherically distributed uncertainty of 5×10^{-12} km/sec^2 in the spacecraft acceleration. The effect on SMAA is that of a constant acceleration of 5×10^{-12}, superimposed on the same 1 mm/sec weighting model. No station location uncertainties are present in this curve.

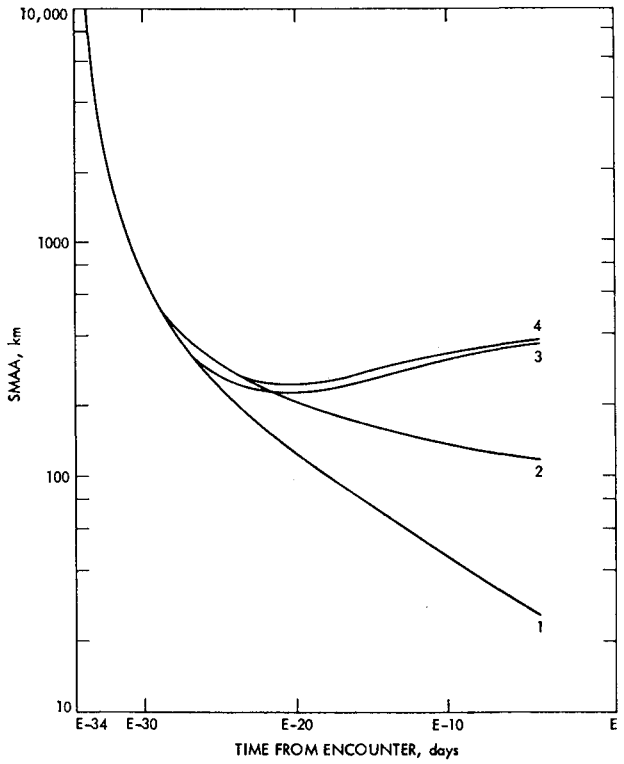

Fig. 6 Navigation accuracy time histories for MM'71.

Curve 4: The top curve represents the total effect of data noise, station location uncertainty, and random nongravitational forces. It is seen that random accelerations dominate in the case of Mariner '71, but that station locations and random forces have approximately an equal effect in 1973.

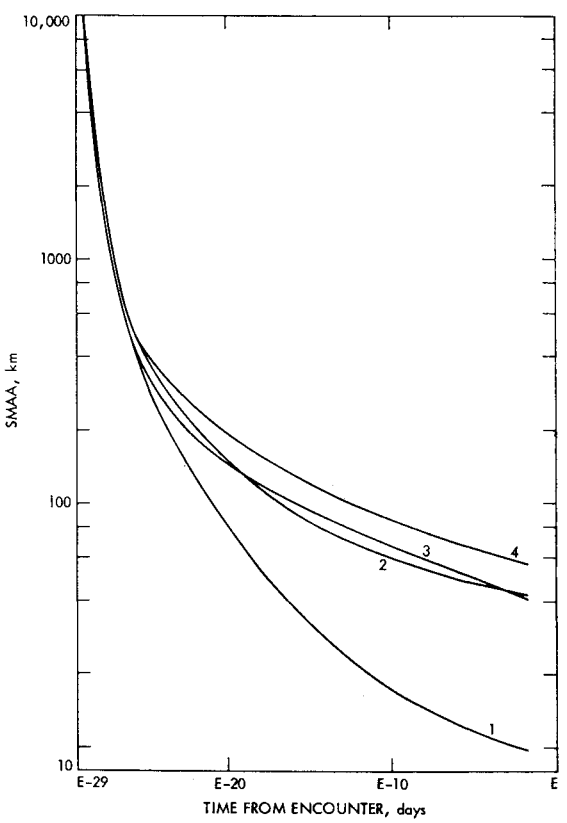

Fig. 7 Navigation accuracy time histories for MVM'73.

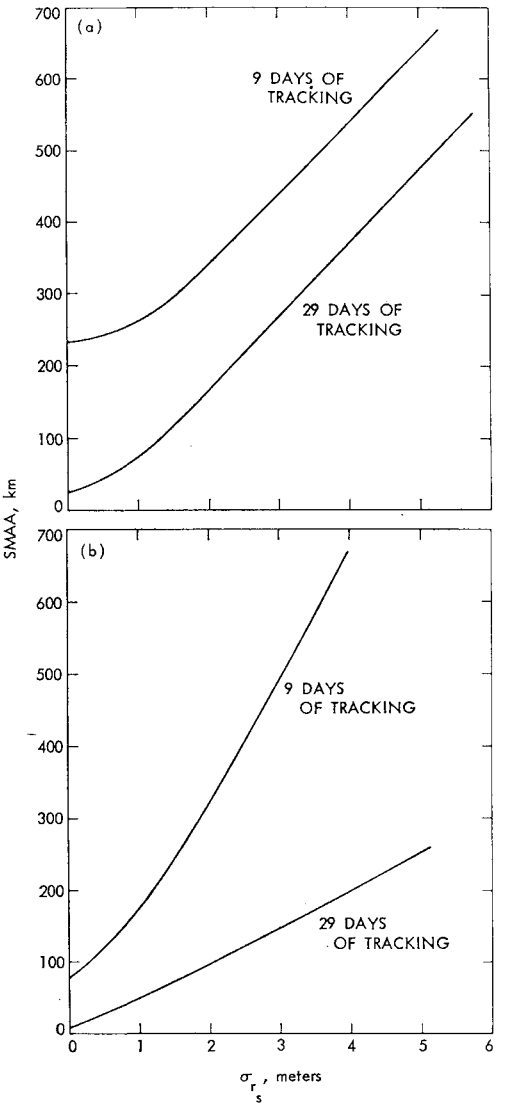

Fig. 8 Sensitivity to station location errors for a) MM'71, and b) MVM'73. Tracking begins at E-34 days ($r_s\sigma_\lambda = 2\sigma_{r_s}$).

The set of curves demonstrates the qualitative difference of the effects of an observer related error source and a spacecraft error source on orbit determination accuracies. Note that for both '71 and '73, the effect of the station location uncertainties is to retard the rate at which information is obtained from the tracking data and limit the terminal accuracy, but that on '71 the effect of an acceleration uncertainty is to actually degrade the navigation accuracy if too much data is taken. The curve for '71 indicates that for accelerations of 5×10^{-2} km/sec^2 the optimum data span is about 15 days, or just half what was plotted, whereas for '73 the solution is still improving after 30 days. This improvement for '73 exists because the ratio of the gravitational attraction force of the sun to the unmodeled force is larger than on the '71 mission.

Sensitivities to the Magnitude of the Error Sources

Figure 8 shows the sensitivities of the two mission accuracies to the magnitude of the station location uncertainties for tracking spans of approximately 9 and 29 days. The assumption is made that longitude uncertainties are twice the spin axis distance uncertainties, i.e., $r_s\sigma_\lambda = 2\sigma_{r_s}$. Comparison of Figs. 8a and 8b, reveals that the 1973 Venus-Mercury mission is much more sensitive than the 1971 mission. The explanation lies in the geocentric declination traces of the

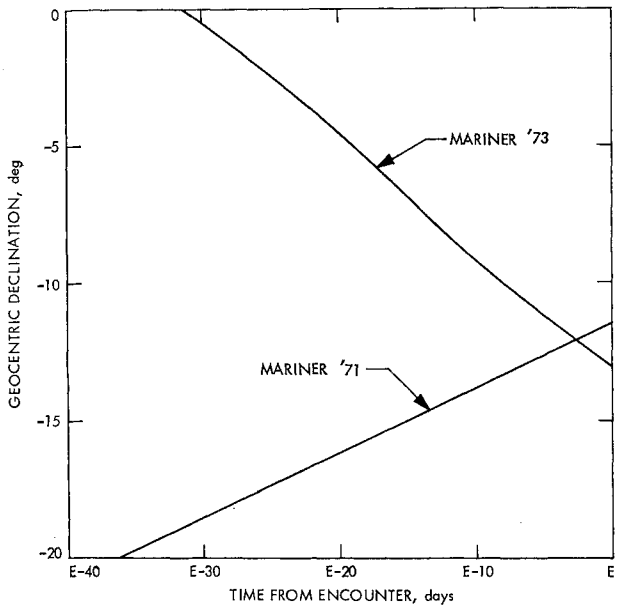

Fig. 9 Geocentric declination of spacecraft vs time for MM'71 and MVM'73.

missions, as shown in Fig. 9. This shows that in the period of interest (the 30 days before planetary encounter) the declination decreases from $-17.5°$ to $-11.5°$ for Mariner '71. In terms of parameters b and c of Eq. (1), this means that near orbit indeterminancy exists at the start of the chosen tracking interval for Mariner '73 because the declination is close to zero. That is, the cidδ_o terms in b and c allow the effect of station location uncertainties to affect the orbit solution maximally.

Figure 10 plots the sensitivities to the magnitude of unmodeled constant accelerations for each mission. MM'71 results appear as a solid line while MVM'73 results appear as a broken line. Here the situation is exactly reversed from

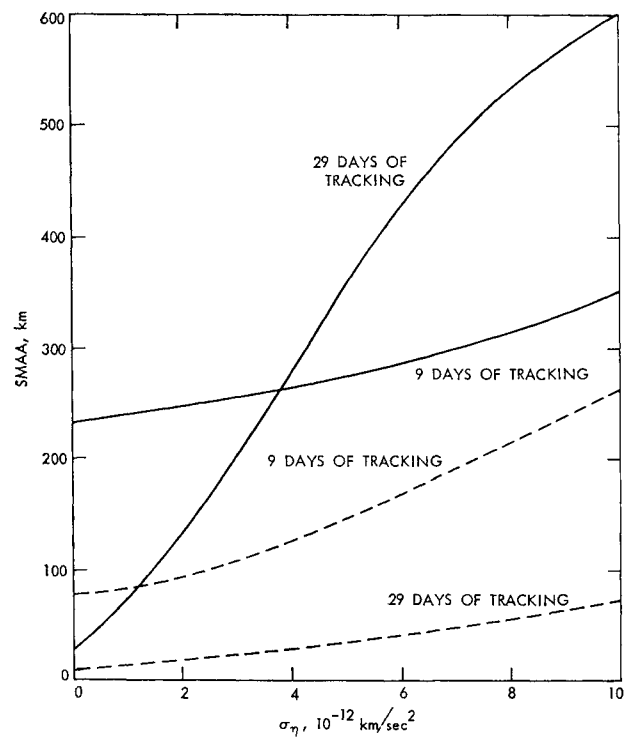

Fig. 10 Sensitivity to unmodeled accelerations for MM'71 and MVM'73.

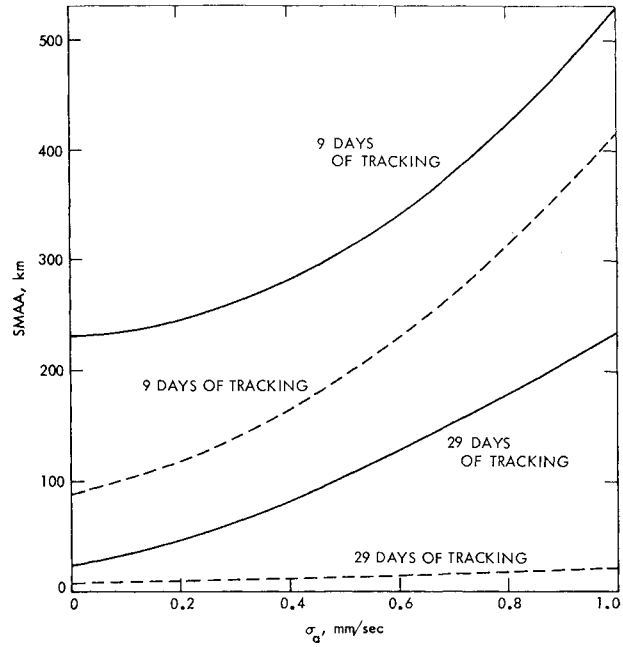

Fig. 11 Sensitivity to unmodeled splace plasma for MM'71 and MVM'73.

that of station location sensitivity. Whereas the '73 curves diverge slightly between the two tracking intervals of 9 and 29 days, they actually cross for '71, which is consistent with the increasing error curve of Fig. 6. The assumption as to the expected magnitude of disturbing forces is seen from Fig. 12 to be critical in the case of Mariner '71, in that below accelerations of 3.8×10^{-12} km/sec^2 the curves do not meet. In fact, at this level the acceleration error curve of Fig. 7 would level off rather than increase. Below this level curve 3 in Fig. 7 would actually decrease between 9 days and 30 days.

Figure 11 plots the sensitivities to the magnitude of the error in the tracking data due to the changing electron content in the space plasma. Although the nominal or expected value of the uncertainty in the parameter a due to the space plasma is just under 0.2 mm/sec for both '71 and '73, and the corresponding degradation in the orbit determination accuracies are small for this level, the curves do illustrate the large degradation which could occur if an abnormally large electron content change is present during the tracking intervals.

B-Plane Position Dispersion Ellipses for the Various Sources

Figures 12 and 13 show the two-dimensional position error ellipses in the B plane resulting from the individual error sources after 29 days of tracking. In these figures the R axis is measured vertically downwards and the T axis is measured horizontally to the right. The effects of the electron content change along the signal path in the Earth's ionosphere is included by considering equivalent station location error as discussed previously. The 1-sigma values of all of the considered parameters used to simulate the error sources in Figs. 12 and 13 are given in Table 1. In all cases, the values listed in Table 1 represent the expected value of the uncertainty of the parameter at the time of the mission.

It is seen from the figures that random accelerations dominate the other error sources for Mariner '71, and station location and ionosphere errors are more important in '73. It is seen also that the major axes of the ellipses are nearly vertical. This is not surprising since the least determined direction is normal to the orbit plane of the probe, which is close to the ecliptic plane for a planetary mission.

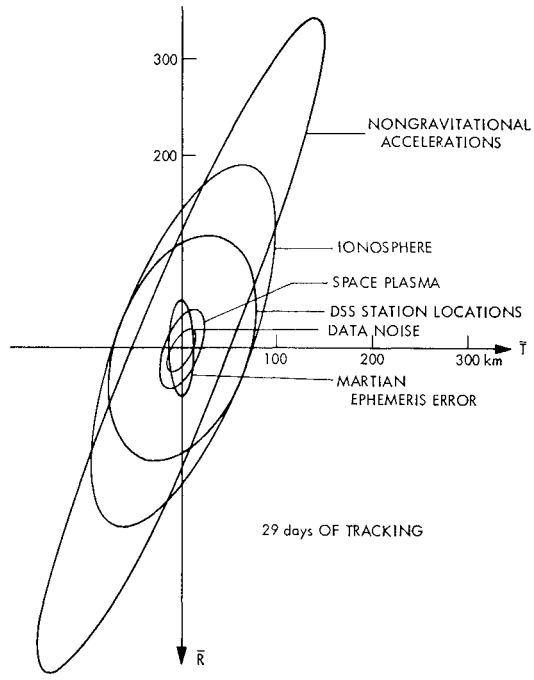

Fig. 12 *B*-plane 1-sigma position dispersion ellipses for MM'71.

Summary

Unmodeled spacecraft accelerations, unmodeled ionosphere, and tracking station location uncertainties all cause navigation inaccuracies greater than those predicted on the basis of 1 mm/sec data noise, nominal unmodeled space plasma, or nominal ephemeris errors.

The effects of several error sources on the navigation accuracies of representative space missions have been presented. The results do not necessarily represent the real-time accuracies which can be obtained during the missions, since more than one station can be used for tracking, ranging data can be employed in the estimation scheme, and the times at which data are given can be selected so as to minimize the navigation errors. In addition, current work in station location determination, ionosphere modeling,[18] and differences range vs integrated doppler techniques[19] will certainly reduce navigation errors on future space missions.

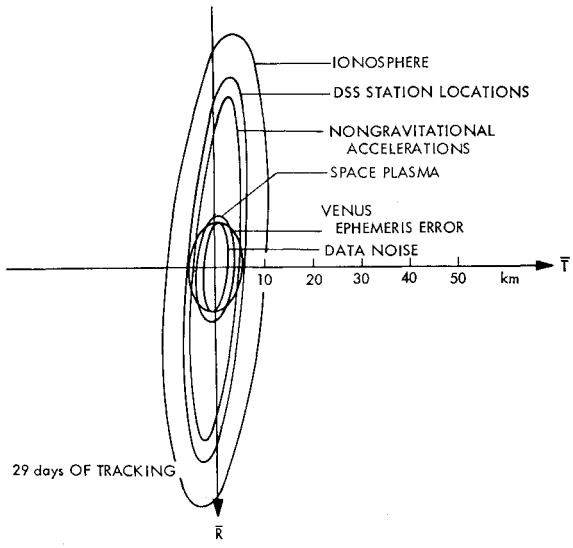

Fig. 13 *B*-plane 1-sigma position dispersion ellipses for MVM'73.

Table 1 Expected 1-sigma parameter uncertainties for MM'71 and MVM'73

Error source	Model parameters	1-sigma uncertainty for MM'71	1-sigma uncertainty for MVM'73
Station physical location	r_s	1.5 m	0.8 m
error	$r_s\Delta\lambda$	3 m	1.6 m
Unmodeled constant acceleration	η	5×10^{-12} km/sec	5×10^{-12} km/sec
Space plasma (Correlation time = 2 hr)	a	0.16 mm/sec	0.16 mm/sec
Ionosphere	a	0.3 mm/sec	0.2 mm/sec
(equivalent station	r_s	2.5 m	1 m
location errors)	$r_s\Delta\lambda$	3 m	2.5 m
Target ephemeris errors	$B \cdot T$	10 km	5 km
	$B \cdot R$	50 km	10 km
Data noise (per 1 min sample)	ϵ	1 mm/sec	1 mm/sec

References

[1] Hamilton, T. W., "Earth-Based Navigation Capabilities of Planetary Missions," presented at the AIAA Guidance and Control Conference, Calif., 1968.

[2] Hamilton, T. W. and Melbourne, W. G., "Information Content of a Single Pass of Doppler Data from a Distant Spacecraft," *Space Programs Summary*, Vol. III, No. 37-39, May 31, 1966, Jet Propulsion Lab., Pasadena, Calif.

[3] Curkendall, D. W. and McReynolds, S. R., "A Simplified Approach for Determining the Information Content of Radio Tracking Data," *Journal of Spacecraft and Rockets*, Vol. 6, No. 5, May 1969, pp. 520-525.

[4] Kalman, R. E., "New Methods and Results in Linear Prediction and Filtering Theory," RIAS TR 61-1, 1961, Martin Marietta Corp., Research Institute for Advance Studies, Baltimore, Md.

[5] Liu, A., "Recent Change to the Tropospheric Refraction Model used in the Reduction of Tracking Data from Deep Space Probes," *Space Programs Summary*, Vol. II, No. 37-50, March 31, 1968, Jet Propulsion Lab., Pasadena, Calif.

[6] Lorell, J., Anderson, J. D., and Sjogren, W. L., "Characteristics and Format of the Tracking Data to be obtained by the NASA Deep Space Instrumentation Facility for Lunar Orbiter," TM. 33-230, June 15, 1965, Jet Propulsion Lab., Pasadena, Calif.

[7] Mulhall, B. D., "Evaluation of the Charged Particle Calibration to Doppler Data by the Hamilton-Melbourne Filter," *Space Programs Summary*, Vol. II, No. 37-57, May 31, 1969, Jet Propulsion Lab., Pasadena, Calif.

[8] Ondrasik, V. J., Mulhall, B. D., and Mottinger, N. A., "A Cursory Examination of the Effect of Space Plasma on Mariner V and Pioneer IX Navigation with Implications for Mariner 1971," *Space Programs Summary*, Vol. II, No. 37-60, Nov. 30, 1969, Jet Propulsion Lab., Pasadena, Calif.

[9] Trask, D. W. and Muller, P. M., "Timing: DSIF Two-Way Doppler Inherent Accuracy Limitations," *Space Programs Summary*, Vol. III, No. 37-39, May 1966, Jet Propulsion Lab., Pasadena, Calif.

[10] Mottinger, N. A., "Status of DSS Location Solutions for Deep Space Probe Missions: Third Generation Orbit Determination Program Solutions for Mariner Mars 1969 Mission," *Space Programs Summary*, Vol III, No. 37-60, Nov. 30, 1969, Jet Propulsion Lab., Pasadena, Calif.

[11] Bourke, R. D., McReynolds, S. R., and Thuleen, K., "Non-Gravitational Forces; Part II: The Mariner V Flight Path and Its Determination From Tracking Data," TR 32-1363, July 1, 1969, Jet Propulsion Lab., Pasadena, Calif.

[12] Pease, G. E., "Orbit Determination from DSIF Tracking Data; Part I: The Mariner V Flight Path and Its Determination from Tracking Data," TR 32-1363, July 1, 1969, Jet Propulsion Lab., Pasadena, Calif.

[13] Lieske, J. et al., "Simultaneous Solution for the Masses of the Principal Planets from Analysis of Optical, Radar, and Radio Tracking Data," presented at the I.A.U. Colloquim No. 9, Heidelberg, Germany, Aug. 1970; also *Celestial Mechanics*, Vol. XI, to be published.

[14] Griffin, R. E. and Sage, A. P., "Large and Small Scale Sensitivity Analysis of Optimum Estimation Algorithms," *IEEE Transactions on Automatic Control*, Vol. AC-13, No. 4, Aug, 1968, pp. 320–329.

[15] Ondrasik, V. J. and Mulhall, B. D., "Estimation of the Ionospheric Effect on the Apparent Location of a Tracking Station," *Space Programs Summary* 37–57, Vol II, Nov. 30, 1969, Jet Propulsion Lab., Pasadena, Calif.

[16] Kingsland, L. and Bollman, W. E., "A Simplified Technique for Estimating the Navigational Accuracy of an Interplanetary Spacecraft," *Journal of Spacecraft and Rockets*, Vol. 7, No. 1, Jan. 1970, pp. 102–105.

[17] Kizner, W. A., "A Method of Describing Miss Distance for Lunar Distance for Lunar and Interplanetary Trajectories," External Publication 674, Aug, 1, 1969, Jet Propulsion Lab., Pasadena, Calif.

[18] Mulhall, B. D., Ondrasik, V. J., and Mottinger, N. A., "Results of Mariner Mars 1969 In-Flight Ionospheric Calibration of Radio Tracking Data," *Space Program Summary*, Vol II, No. 37–60, Nov. 30, 1969, pp. 76–77, Jet Propulsion Lab., Pasadena, Calif.

[19] McDoran, P. F. and Wimberly, R. N., "Charged Particle Calibration from Differenced Range Versus Integrated Doppler—Preliminary Results from Mariner Mars 1969," *Space Program Summary*, Vol. II, No. 37–58, pp. 73–77, July 31, 1969, Jet Propulsion Lab., Pasadena, Calif.